Atomic Arrangement of Iodine Atoms inside Single-Walled Carbon Nanotubes

X. Fan,[1,2] E. C. Dickey,[1,*] P. C. Eklund,[3,†] K. A. Williams,[3] L. Grigorian,[3,‡] R. Buczko,[2,4,§]

S. T. Pantelides,[4,2] and S. J. Pennycook[2]

[1]*Department of Chemical and Materials Engineering, University of Kentucky, Lexington, Kentucky 40506*
[2]*Solid State Division, Oak Ridge National Laboratory, Oak Ridge, Tennessee 37831*
[3]*Department of Physics and Astronomy, University of Kentucky, Lexington, Kentucky 40506*
[4]*Department of Physics and Astronomy, Vanderbilt University, Nashville, Tennessee 37235*
(Received 9 November 1999)

We report atomic resolution Z-contrast scanning transmission electron microscopy images that reveal the incorporation of I atoms in the form of helical chains inside single-walled carbon nanotubes. Density functional calculations and topological considerations provide a consistent interpretation of the experimental data. Charge transfer between the nanotube walls and the I chains is associated with the intercalation.

Single-walled carbon nanotubes (SWNTs) have been shown to be amphoteric in character; i.e., they can exchange electrons with a dopant atom (or molecule) to form the corresponding positively or negatively charged counterion [1,2]. Little is known, however, about the actual dopant sites and distributions. In this Letter, we present Z-contrast scanning transmission electron microscopy (STEM) images and complementary theoretical calculations that reveal the distribution of I atoms within I-doped SWNT bundles.

SWNT ropes were made by an arc-discharge technique [3] and doped by immersion into molten iodine as described previously [4]. The intercalation was found to be reversible and Raman scattering showed charged polyiodide ions to be distributed throughout the bundles [4]. It has been generally assumed that the intercalant enters the interstitial channels between tubes. This assumption was based on the belief that the ends of the as-prepared tubes are closed, unless opened by a postsynthesis treatment, e.g., refluxing in concentrated acid [5,6]. Here we report Z-contrast images of individual SWNTs protruding from the ends of SWNT bundles that reveal iodine chains to be incorporated inside the tubes. Images were taken with a VG microscopes HB603U STEM, operating at 300 kV, equipped with a high-resolution objective lens capable of forming a probe 0.13 nm in diameter. This microscope has demonstrated information transfer in Z-contrast images at the sub-angstrom level [7] and direct imaging of individual heavy atoms on a light support [8]. Of particular relevance to this work is the fact that the Rutherford scattering used to form Z-contrast images scales with the square of the atomic number [9] resulting in large contrast between I ($Z = 53$) and C ($Z = 6$). To reduce the noise in some of the images, maximum entropy refinement was utilized [10–12].

In order to guide interpretation of the experimental data, we performed a number of theoretical calculations using density functional theory with the local density approximation of exchange correlation, norm-conserving pseu-

dopotential plane waves, and supercells [13]. The use of complete nanotube supercells was impractical because of the large number of atoms required. Calculations were therefore performed for free I chains and for I chains on flat graphene sheets or on graphene sheets that were bent to simulate the curvature of the interior of a nanotube.

Figure 1 compares bright field and Z-contrast images from regions in the sample where several individual tubes can be distinguished. Whereas the bright field image shows very little contrast and is ambiguous as to the position or even presence of I, the dark field image directly reveals the projected I distribution. Comparing the two images, it is seen that the iodine is incorporated within one particular nanotube (labeled A) but is not present in others in the bundle (e.g., nanotube B). The diameter of the A tube is 1.36 nm and assuming that the π electrons extend 0.17 nm from the wall, as in graphite, the inner tube diameter would be $\approx$1.03 nm. From the width of the bright stripe, 0.65 nm, it is clear that the iodine is incorporated inside the single-walled tube.

The internal iodine is confirmed in the higher resolution Z-contrast images of Figs. 2 and 3, where two chains of iodine atoms are observed inside the nanotubes. The projected spacing between the two chains is observed to modulate along the tube axis, suggesting that the chains have a helical structure in three dimensions. The period of the modulation is measured to be about 5 nm in Fig. 2, but other tubes show different periodicities. For example, Fig. 3(a) shows a tube containing a double helix with a periodicity of about 12.5 nm, and Fig. 3(b) shows a double helix with an even longer periodicity. The observation of different periodicities suggests that the iodine chains adopt a preferred orientation with respect to the nanotube wall, and the different periods correspond to tubes with different chirality. Direct attempts to confirm the chirality of individual tubes by electron nanodiffraction were unsuccessful, however.

The observed discontinuities and variations in intensities along the length of the iodine chains hamper direct
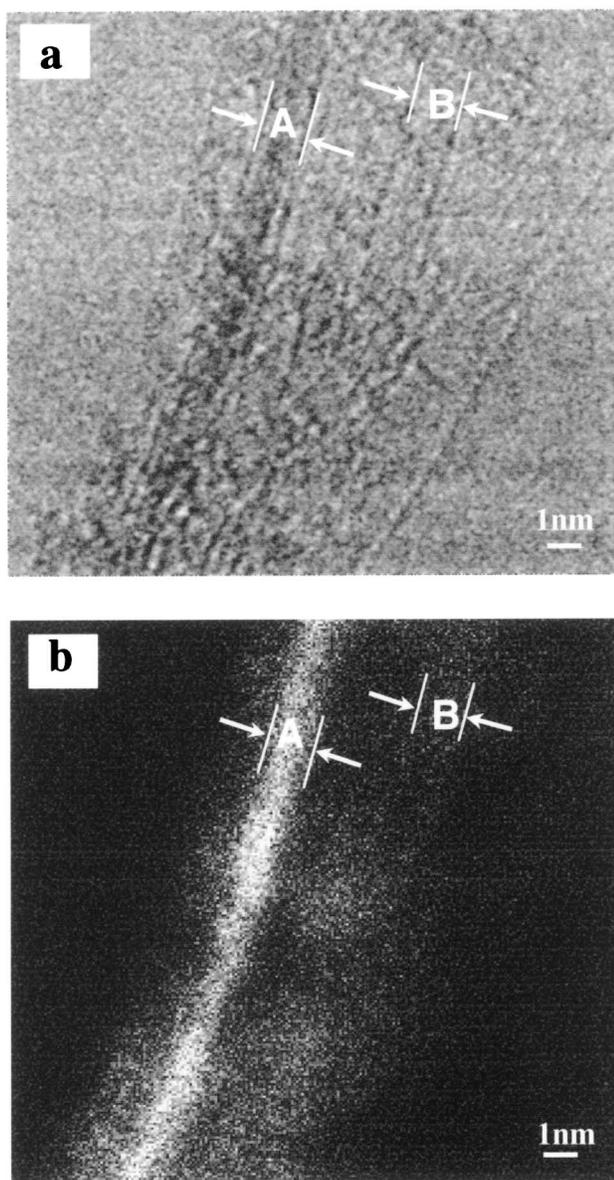
FIG. 1.   (a) Bright field phase contrast image and (b) dark field Z-contrast image of a SWNT rope, taken simultaneously on the STEM.   The conventional phase contrast image is useful for locating the nanotube walls; the precise registry of the two images therefore allows the iodine distribution to be determined to high precision. Iodine is clearly inside some tubes, such as A but not others, for example, B.

FIG. 2.   (a) Higher resolution Z-contrast image of a SWNT containing two strands of iodine. (b) Maximum entropy processed image to reduce the noise. Two constrictions can be seen, consistent with the projection of a double helix configuration with the two chains spiraling along the inside walls of the nanotube as shown in the overlay in (c). The period of the helix is about 5 nm, and the maximum separation of the two strands is ~0.65 nm, much less than the 1.3–1.4 nm diameter of the SWNT.

structure determination. These intensity variations are believed to result from electron displacement damage, which occurs during the imaging process. Since we are imaging single atoms, and not columns of atoms as in crystalline materials, displacements of individual atoms have more severe consequences for the image resolution. The maximum energy transferred from the incident electrons to the iodine nucleus, T_m, assuming a relativistic elastic collision between the electron and a stationary nucleus is 3.3 eV for 300 keV electrons incident on an I atom [14,15]. The energy barrier necessary to remove an iodine atom from
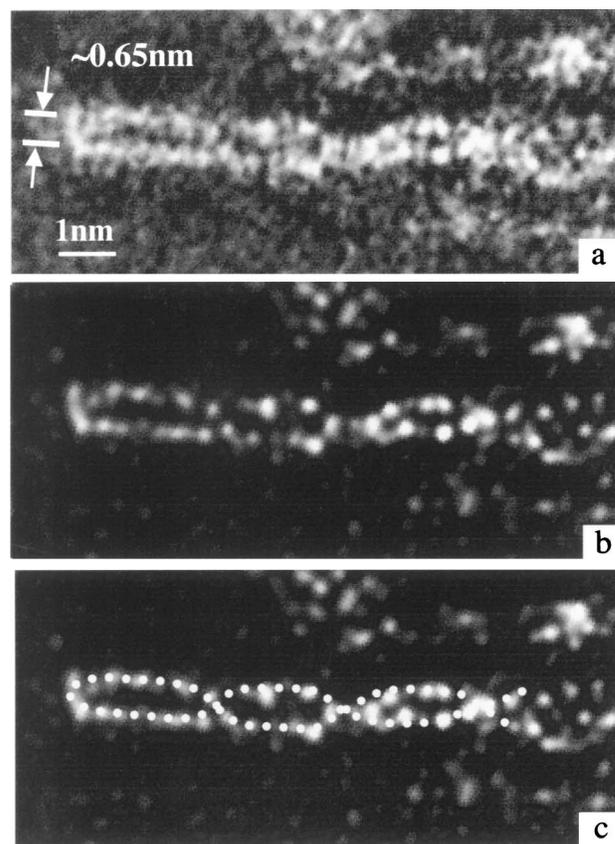
an I_3^- chain was calculated to be ~1.5 eV by first-principles total energy calculations. Taking into account the 0.3 eV/atom binding energy of the chain to the tube wall (to be discussed in detail below), we place an upper estimate on the displacement energy (E_d), or the energy necessary to displace an I atom from the chain, of 1.8 eV. Since $E_d/T_m \sim 0.5$ significant beam damage will occur during the imaging process. These atomic displacements lead to increased noise and thus variations in projected positions and intensities, which are apparent in Figs. 2 and 3.

To guide interpretation of the experimental data, we performed several first-principles calculations that shed light on interactions between iodine and the nanotube wall. Similar continuous, one-dimensional iodine structures to those observed in this study have been reported in the polymer literature where iodine has been used to increase the electrical conductivity of polymers by orders of magnitude [16–18]. Diffraction studies of iodine-doped polymers indicate that the iodine intercalates the one-dimensional
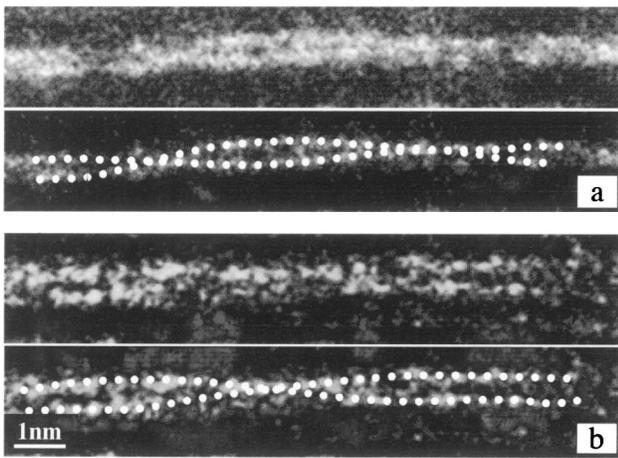
FIG. 3.   Images of iodine doped SWNT ropes showing different periodicities, shown schematically above the tubes; (a) an iodine helix showing 12–13 nm periodicity; (b) a helix of longer periodicity.

interstitial channels of crystalline polymers in the form of continuous linear arrays. Furthermore, Raman spectroscopy shows the charge transfer to the iodine to be typically 0.33 eV/iodine or 0.2 eV/iodine, corresponding to I_3^- and I_5^- species, respectively [16–18]. Since we observe similar linear arrays of iodine and, as reported earlier [4], the Raman modes of the I-doped SWNTs agree with those reported for the I_3^- and $(I_5)^-$ arrays [16–18], we conclude that the iodine is in a similar state to that found in doped crystalline polymers. We therefore performed calculations for chains of three and five iodine atoms above both a flat graphene sheet and a curved sheet, as illustrated by Fig. 4. This configuration would correspond to one unit cell of the continuous iodine chain. In all cases, we found an equilibrium distance of ~ 0.35 nm between the I chain and graphene sheet with a net binding of ~ 0.3 eV per I atom, provided the initial position of the I chain was close enough to the graphene sheet to allow charge transfer to take place. The chain prefers a straight configuration. We contrast this finding with the fact that neutral chains of three I atoms in free space are bent whereas charged chains are straight. We conclude that charge transfer from the tube wall to the I chain stabilizes the I chains. Our calculated equilibrium distance (0.35 nm) agrees precisely with the distance obtained from the observed 0.65 nm spacing of the chains in Fig. 2, if we assume the double helix is located inside a $(10, 10)$ tube of 1.36 nm diameter.

Another indication of the influence of the curved nanotube walls on the formation of the helical chains is provided by the topological considerations. I_2 does not intercalate graphite because of its large van der Waals diameter (0.396 nm) [17] and its 0.27 nm interatomic spacing does not correlate with any spacing in the basal plane of graphite [19–21]. However, the space available for intercalation is much greater in nanotubes and the radially projected interatomic spacings of *curved* graphene

sheets better match the preferred I-I spacing. $(10, 10)$ tubes are thought to be a common type of nanotube in the arc-derived material, and in Fig. 4 we show three possible correlations between the nanotube lattice and the iodine spacings, which are nearly commensurate. Continuous chains bound to these sites result in helical arrangements with periods of 12.5, 5, and 1.5 nm. First-principles calculations show the I chains to be stable in these commensurate orientations. The longest two periods for the $(10, 10)$ tube are in excellent agreement with the helices imaged in Figs. 3(b) and 2. The shorter period helix would project as a rather uniform arrangement of iodine, which may explain images of the type shown in Fig. 1(b). A complete structural model for a $(10, 10)$ tube with a 5 nm double helix of iodine inside is given in Fig. 5. Although we have focused our discussion on $(10, 10)$ tubes because of their relatively simple, symmetric structure, typical nanotube samples are believed to have a distribution of diameters and chiralities. Tubes with different chirality would, of course, be expected to show different chain periodicities because of the importance of the chain-(tube wall) interaction.

Two continuous strands of iodine with the 5 nm period give a composition of IC_{20}, but it would appear feasible to incorporate additional spirals of iodine, up to five before the distance between neighboring strands become too close, giving a composition IC_8. This provides an alternative explanation for the lack of an observed helical structure in Fig. 1(b). For the 1.5 nm helix there would be sufficient room for only two chains, giving a saturation doping of IC_{15}. The overall composition determined experimentally by weight uptake measurements and thermogravimetric analysis is IC_{12} [4], but since we observe many tubes to be unfilled, this suggests substantial iodine is also incorporated in the interstitial positions between tubes in a bundle. We would anticipate that polyiodide chains in the
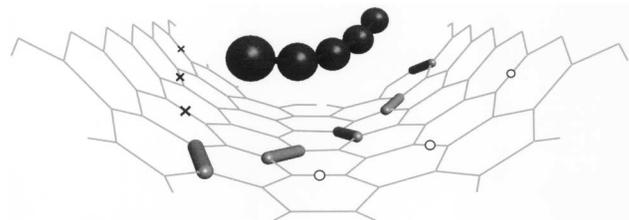

FIG. 4.   Bent graphene sheet used in the calculations with periodic boundary conditions. The curvature corresponds to the correct curvature of an actual $(10, 10)$ nanotube. The distances between the C-C bonds that are highlighted with rods 3.2 Å) project radially to 0.28 nm, very close to the preferred I-I spacing of 0.29 nm, at a distance of 0.35 nm where the I chain prefers to rest. This results in a helical arrangement of iodine with a 5 nm period, as seen in Fig. 2. Two other near-commensurate directions are possible. The direction marked by crosses has an I-I spacing of 0.31 nm and a period of 12.5 nm, as seen in Fig. 3(a). The direction shown by circles has an I-I spacing of 0.30 nm and a much shorter period, 1.5 nm.
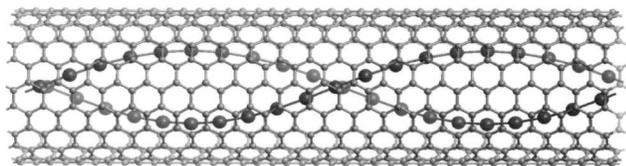
a
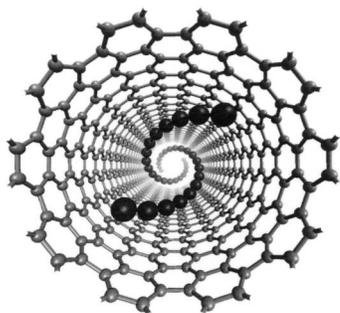
b

FIG. 5.   Structure model obtained by extrapolating the 5 nm helix of Fig. 4 to a full scale $(10, 10)$ nanotube, (a) side view and (b) top view.

interstitial locations between tubes could bond by a similar mechanism although for $(10, 10)$ armchair tubes there are no good correlations with the projected nanotube lattice.

It is interesting to note that previous studies did not observe any charge transfer between SWNTs and iodine when the iodine was present in the vapor phase [2]. Molten iodine is quite different from iodine vapor. In particular, iodine molecules in molten iodine tend to dissociate into highly reactive iodinium (I^+) and polyiodide $(I_3)^-$ species [22]. On the other hand, the iodine vapor contains only nondissociated iodine molecules, which are less chemically active as compared to ionic forms. The (I^+) ions in the molten I are very strong oxidizing agents and could attack the remaining catalyst particles at the tube ends or the defect sites in the tube walls. These sites could subsequently serve as entry points for the polyiodide species. Although we have no conclusive evidence for this intercalation mechanism, x-ray diffraction spectra from the samples do show all of the metal catalyst to be oxidized to their metal-iodide phases. We do not yet understand why some of the tubes are intercalated and others are not. Such understanding awaits more thorough understanding of the tube end structures.

*To whom correspondence should be addressed. Electronic address: ecdickey@engr.uky.edu

†Current address: 104 Davey Laboratory, The Pennsylvania State University, University Park, PA 16802-6300.

‡Current address: Fundamental Research Lab, Honda R&D Americas, Inc., 100 Town Center, Suite 2050, Southfield, MI 48075.

§Permanent address: Institute of Physics, Polish Academy of Sciences, 02-668, Warsaw, Poland.

[1] R. S. Lee, H. J. Kim, J. E. Fischer, A. Thess, and R. E. Smalley, Nature (London) **388**, 255 (1997).

[2] A. M. Rao, P. C. Eklund, S. Bandow, A. Thess, and R. E. Smalley, Nature (London) **388**, 257 (1997).

[3] C. Journet et al., Nature (London) **388**, 756 (1997).

[4] L. Grigorian, K. A. Williams, S. Fang, G. U. Sumanasekera, A. L. Loper, E. C. Dickey, S. J. Pennycook, and P. C. Eklund, Phys. Rev. Lett. **80**, 5560 (1998).

[5] J. Liu et al., Science **280**, 1253 (1998).

[6] J. Sloan et al., Chem. Commun. **3**, 347 (1998).

[7] P. D. Nellist and S. J. Pennycook, Phys. Rev. Lett. **81**, 4156 (1998).

[8] P. D. Nellist and S. J. Pennycook, Science **274**, 413 (1996).

[9] D. E. Jesson and S. J. Pennycook, Proc. R. Soc. London A **449**, 273 (1995).

[10] S. F. Gull and G. J. Daniell, Nature (London) **272**, 686 (1978).

[11] S. F. Gull and J. Skilling, IEE Proc. F, Radar Signal Process. **131**, 646 (1984).

[12] A. J. McGibbon, S. J. Pennycook, and D. E. Jesson, J. Microsc. **195**, 44 (1999).

[13] P. Hohenberg and W. Kohn, Phys. Rev. **140**, B1133 (1964).

[14] L. Reimer, Transmission Electron Microscopy (Springer-Verlag, New York, 1993), Chap. 5.

[15] A. Maiti, M. F. Chisholm, S. J. Pennycook, and S. T. Pantelides, Appl. Phys. Lett. **75**, 2380 (1999).

[16] R. C. Teitelbaum, S. L. Ruby, and T. J. Marks, J. Am. Chem. Soc. **101**, 7568 (1979).

[17] B. H. Baughman et al., in Molecular Metals, edited by W. E. Hatfield (Plenum Press, New York, 1979), p. 187.

[18] M. J. Nilges, E. K. Barefield, R. L. Belford, and P. H. Davis, J. Am. Chem. Soc. **99**, 749 (1977).

[19] S. Nakashima et al., Chem. Phys. Lett. **268**, 359 (1997).

[20] H. Werner, M. Wesemann, and R. Schlogl, Europhys. Lett. **20**, 107 (1992).

[21] S. Flandrois, C. Hauw, and B. François, J. Phys. (Paris) **44**, C3-523 (1983).

[22] S. A. Jenekhe, S. T. Wellinghoff, and J. F. Reed, Mol. Cryst. Liq. Cryst. **105**, 175 (1984).